IEEE Access
Multidisciplinary | Rapid Review | Open Access Journal

Received 11 September 2023, accepted 15 September 2023, date of publication 25 September 2023,
date of current version 4 October 2023.

Digital Object Identifier 10.1109/ACCESS.2023.3319076

RESEARCH ARTICLE

Multi-Layer and Multi-Channel Dynamic Routing Planning and Initial Point Positioning of Weld Seam Based on Machine Vision

TONG LI AND JIANG ZHENG
School of Materials Science and Engineering, Xihua University, Chengdu 610039, China
Corresponding author: Tong Li (lit072511@163.com)

ABSTRACT The welding process for medium and thick plates typically involves multi-layering and multi-channeling, but its quality and reliability require further improvement. Therefore, this study introduces the convolution neural network algorithm to establish a deep learning model for weld seam recognition. Additionally, the structured light imaging method is used to accurately position the V-shaped weld groove. Meanwhile, a machine vision based multi-layer and multi-pass dynamic routing planning algorithm was also studied and designed, and a contour feature point recognition algorithm for the filling layer was developed. Thus, dynamic routing planning is achieved. It is demonstrated that the difference between the coordinates acquired by the deep learning model and the ideal region decreases steadily and reaches a minimum of (200,80). The confidence level of weld seam detection gradually increases with the adjustment of the welding robot, reaching a maximum of 98%. The confidence level of the detected feature points reaches 100%. In the meantime, the remaining height of the fusion after welding is 2.5mm. There are no negative phenomena present on the surface of the weld seam, meeting the necessary process requirements. Such discrepancies as undercut, incomplete penetration, slag inclusion, and porosity are absent. It shows that the welding technology based on machine vision has strong feasibility, effectively improves the automation level and efficiency of welding technology, and provides reliable technical support for the development of modern machine vision welding technology.

INDEX TERMS Machine vision, multiple layers and channels, initial point positioning, dynamic lane arrangement, welding, machine learning algorithms, robot vision systems.

I. INTRODUCTION

Welding is an important manufacturing process, and the quality of the weld seam is directly related to the strength and reliability of the welded part. Further development of robotics can focus on research in dynamic nesting planning, weld initial point localization, robot path planning and trajectory tracking. The aim is to improve the quality and accuracy of the weld seam, reduce the distortion rate, and minimize the effect of ambient light on weld seam localization [1]. Currently, vision sensors are mostly used in automatic weld seam path tracking for welding robots. In the multi-layer multi-pass scheduling problem, the traditional way is mainly to obtain the trajectory of the filler weld by offsetting the weld path. Although this method is relatively straightforward to use and enhances welding efficiency, it is vulnerable to weldment deformation resulting from the high temperature. Therefore, the method of filling directly following the trajectory may not be able to guarantee the welding quality [2], [3]. In addition, although traditional machine vision methods can enhance the accuracy of initial weld seam localization, they may be sensitive to ambient lighting during welding, thereby resulting in error amplification. This may adversely affect the quality of the weld. In further developing work on robotics, attention could be given to the research on dynamic nesting planning, weld initial point localisation, robot path planning and trajectory tracking. Thus improving weld quality and accuracy, reducing the rate of distortion and the effect of ambient light on weld positioning. These studies will help to further improve the automation and efficiency of welding technology. Therefore, the study suggests implementing machine vision algorithms to dynamically extract suitable

The associate editor coordinating the review of this manuscript and approving it for publication was Antonio J. R. Neves.

parameters for adjusting the weld trajectory to enhance filler quality. At the same time, the weld recognition deep learning model is used for rough positioning of the weld position. The machine vision algorithms accurately locate the starting point of the weld to improve welding quality and efficiency, and to advance the automation and intelligence of welding technology [4], [5]. The research mainly includes four parts. The first part mainly reviews the existing welding methods for multi-pass welds at home and abroad. The second part is mainly based on the processing method of machine vision algorithm to study the initial point positioning of the weld seam and the dynamic scheduling method of multi-layer multi-pass welding of medium-thick plate. Among them, in the first section, a deep learning model for recognising V-shaped bevels is mainly trained using the convolutional neural network algorithm. And the image processing algorithm for the weld's feature points is composed utilizing the machine vision processing technique to attain the initial location of the weld. This approach empowers the welding robot to autonomously identify the initial position point of the weld under a vast field of view. In the second section, a dynamic scheduling algorithm for multi-layer multi-pass welding of medium-thick plates is presented by analyzing the welding robot's multi-layer multi-pass welding method. The system can modify welding parameters while welding and capture contour images during multi-layer, multi-pass welding to recognize characteristic points of the weld contour. It then updates the welding position based on the remaining width and height information of the weld bevel in real time. In the third part, the performance advantages of the machine vision-based multi-layer multi-pass dynamic lane planning algorithm and the initial point positioning algorithm are verified. The fourth part of the paper summarises and discusses the proposed methods and experimental results, and presents the current shortcomings and future prospects. The contribution of this article lies in the introduction of machine vision algorithms to extract parameters such as the remaining filling height of the weld seam and the remaining width of the weld layer, based on the original path offset method. The extraction of these parameters is dynamic and can be adjusted based on real-time welding conditions. Secondly, a machine vision based structured light vision algorithm is used for initial positioning of welding points. Compared to currently more advanced stereo vision algorithms, this algorithm displays smaller deviation values in the initial positioning of welding points and presents significant performance advantages. Finally, by dynamically adjusting the welding trajectory and extracting parameters based on machine vision algorithms, the filling quality of multi-layer and multi-pass welding can be improved.

II. RELATED WORKS

The welding problem of multiple welds has always been a hot topic in the industrial field. Scholars such as S.Trupiano have found that simulating multi-layer and multi pass welds using traditional 3D models is time-consuming. Therefore, a new equivalent parametric modeling method has been proposed to simulate longitudinal multi pass welds. This model can detect the local deformation and residual stress of welds, utilizing the steady-state structural analysis method. Compared to traditional 3D numerical models, this welding modeling method reduces the calculation time by about 10 times [6]. R.K.W.Vithanage et al. have used the maximum inter-class variance method for the extraction of laser beam contours in images for a multilayer multi-pass welding problem. The center of mass for the laser line contour is determined by column and linear regression is used to optimize the contour line. The adaptive slope detection algorithm is utilized to locate the image laser jump between the weld seam and the weld plate, facilitating the detection of the weld seam's left and right boundaries, which subsequently leads to the identification of the weld seam. The results show that the algorithm can be applied to the guidance of the weld start position, and has a high recognition accuracy [7]. M.Zhu et al. believed that the control and prediction of residual stress can provide a more complete structural evaluation of welded joints. Therefore, a method combining finite element analysis with practical application was proposed and the effecting of welding sequence on ML-MC welded joints was explored. The welding sequence has a small impact on the peak residual stress, but huge in the longitudinal residual stress inside the joint [8]. Y.Han's team proposed the integral robust control algorithm for the planning and tracking of welding paths. Through image processing and analysis of the workpiece, the information regarding the area and path to be welded is determined. The results showed that the algorithm can effectively automate the welding process and improve the welding quality [9]. A.Sarmat et al. proposed a neural adaptive learning algorithm for constrained nonlinear systems with disturbance suppression to further improve the control performance and robustness of welding robots. The algorithm can employ a neural network to estimate the system's nonlinear mapping relationship, and execute online learning and parameter modification based on the error signal to accomplish disturbance suppression and asymptotic tracking of the system. The results indicated that it contributes to the suppression and adaptive adjustment of system disturbances and disturbances [10]. Scholars such as M.Shahabi believed that the V-shaped groove joint of intersecting pipelines needs to be filled with multi-layer welding, but it increased the complexity of the problem. Therefore, the team proposed a multi-layer welding method for pipelines with intersecting rear walls. This method effectively fills the joint space of the V-shaped groove around the pipeline, and the path planning method has good robustness [11].

L.H. Guilherme et al. wrote a set of welding robot trajectory planning software for the trajectory planning problem in the multilayer-multipass welding process of industrial robots. It determines the machine welding position parameters for each weld pass through a multi-layer-multi-pass welding method in which the user manually sets the welding position

points and the number of weld passes. The software obtained better welding results in welding tests [12]. Y. He et al. processed image information by laser-assisted vision. They used a distance filtering method to recognize the image feature point information of weld contour in multi-layer multi-pass welding process. The method provides a reference for the weld width recognition algorithm in multi-layer multi-pass scheduling planning. The results showed that the inflection point identification of the bottom of the weld groove plays a certain reference role in the process of measuring the weld depth [13]. To address the sensitivity of cold cracking in steel structure welding manufacturing, N.MukMukai's team proposed a new welding process and applied it to window constrained welding cracking experiments. The content of metallic hydrogen under this process was greatly reduced, which has a good effect of preventing cold cracking and reduces the preheating temperature of about 50°C [14]. To effectively monitor the safety status of oil pipelines, scholars such as Hasan have designed a numerical simulation method for residual stress states in multiple weld seams. It calculated the residual stress distribution, temperature and hardness distribution of multi pass welding through two-dimensional thermal finite element model, and takes temperature dependence as an important factor to consider. The results showed that the simulation results have a high degree of consistency with the test results, which can save time [15]. P.Asadi's team raised a non coupled thermal 3D model for numerical analysis of residual stress. It was capable of designing circular welding around pipelines. The simulation results showed that as the welding speed gradually increases, the axial tensile stress on the pipeline surface shows a decreasing trend, proving the effectiveness of this model [16].

In summary, many researchers in the industry have conducted extensive research on the welding methods of multiple welds, and many of them have combined them with visual algorithms for weld detection and welding. But its main approach is to first obtain the size of the weld seam and then set the welding path, which is easily affected by temperature and causes deformation of the original path. Therefore, in this project, machine vision algorithms were used for dynamic welding of welds to achieve good application results in actual ML-MC welding.

III. ML-MC WELDING PLANNING AND INITIAL WELDING POINT POSITIONING BUILT ON MACHINE VISION

Welding robot is a robotic system that automatically performs welding tasks with high precision, efficiency and consistency. With the development of industrial automation and intelligence, welding robots are widely used in the manufacturing industry. Multi-layer multi-pass dynamic lane planning is to automatically plan the welding path and lane sequence according to the shape and requirements of the weld seam. The machine vision system inspects the weld seam to gather information on its position, shape, and size to facilitate path planning and lane optimization. This method

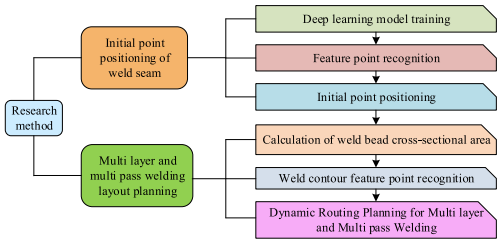

FIGURE 1. The structural schematic diagram of YOLOv3.

is suitable for complex welding processes and multi-layer multi-pass tasks to improve welding efficiency. Welding robots have a wide range of application prospects in industrial manufacturing. Through multi-layer multi-pass dynamic path planning and weld initial point localization based on machine vision, it improves welding quality and precision, reduces deformation rate, and promotes the development of automation and intelligence of welding technology. The paper aims to provide efficient, reliable and flexible welding solutions for the manufacturing industry. This chapter will focus on the specific implementation steps and application effects of machine vision algorithms in the positioning of the initial point of welding and multi-layer multi-pass platoon welding planning [17], [18]. The schematic diagram of the research method in the paper is shown in the figure 1.

A. MACHINE VISION BASED INITIAL POSITION POINT LOCATION TECHNOLOGY FOR WELDS

1) TARGET IDENTIFICATION AND DETECTION ALGORITHM BASED ON CONVOLUTIONAL NEURAL NETWORK

In the process of identifying weld seams, the use of deep learning (DL) object detection algorithm can more accurately identify the type and location of the weld seam. Therefore, the Convolutional neural network (CNN) target detection algorithm is proposed to locate the initial position of the weld. The CNN structure mainly includes convolutional, input, fully connected, excitation and pooling layer. Among them, the role of pooling layer is to select features, thereby reducing the number of features. The fully connected layer mainly achieves dimensionality reduction of local features, and performs classification and regression processing on them. In addition, because the majority of the gathered data displays a non-linear distribution, the study incorporated a Rectified Linear Unit (ReLU). This technique is able to successfully address the issue of gradient vanishing during CNN computation, resulting in the effective training of deep networks. The calculation of the ReLU function is Equation (1).

$$\sigma(x) = \max(0, x) = \begin{cases} 0, & x < 0 \\ x, & x \geq 0 \end{cases} \tag{1}$$

To ensure accurate recognition of welds in a large field of view, the YOLOv3 algorithm was used to train the DL model. YOLO primarily partitions the image into multiple regions and employs CNN to operate on images within the same

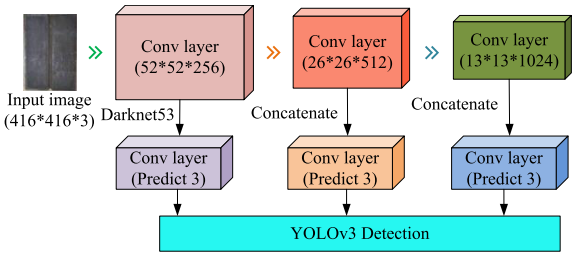

FIGURE 2. The structural schematic diagram of YOLOv3 is shown in the figure.

region, simultaneously assessing the image's confidence level. Next, it selects the regions that meet the confidence requirements to obtain the location information of the detection target. Compared with YOLOv1 and YOLOv2 algorithms, YOLOv3 has a faster detection speed. The network structure consists of 106 convolutional layers. The initial 53 convolutional layers were utilized for network pre-training, whereas the remaining 53 convolutional layers were used for formal training. Meanwhile, the algorithm includes three detections. Among them, the algorithm performs the first detection at layer 82, with a step size of 32 and the generated feature map size of 13 × 13, which mainly used for detecting larger target objects. The algorithm performs a second detection at layer 94, with a step size of 16 and generating a size of 26 × 26 images, mainly used for detecting medium sized images. The algorithm performs the third detection on layer 106, with a step of 8 and a generated image size of 52 × 52, mainly used for detecting smaller target objects [19]. Figure 2 is a schematic diagram of the structure of YOLOv3.

2) INITIAL POINT POSITIONING OF WELD SEAM BASED ON IMAGE PROCESSING ALGORITHM

The cross-section of the V-shaped weld groove of a welded component has several corner features, which are called the characteristic points of the groove. This includes the left edge, right edge, and bottom feature points. The schematic diagram of the V-shaped weld groove is exhibited in Fig.3(a). The identify method for feature points mainly adopts image processing algorithms. The algorithm saves the coordinate positions of the three feature points of the weld and analyzes their spatial relationships, enabling accurate classification of whether the current structured light's captured target object belongs to the V-groove. Next, the laser image of the weld seam read by the camera undergoes image preprocessing which includes extraction of the Region of Interest (ROI) region, gray scale processing of the ROI region image, and threshold segmentation for extracting the contour line image of the weld seam. Finally, the image of the weld seam area is trimmed using morphological processing and combined with stripe refinement and other operations to extract the centerline position of the laser stripe. The effect of extracting ROI regions from the image is shown in Fig.3(b). The research mainly analyzes the V-groove of the weld, and processes the

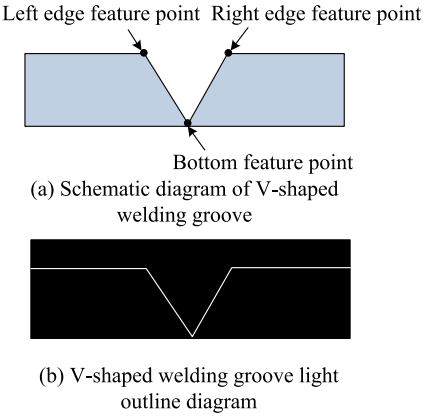

FIGURE 3. Diagram of V-shaped weld groove.

structured light contour image of the weld to identify the feature point information of the V-groove [20].

The image processing method involves several steps. Firstly, the welding image captured by the camera needs to be preprocessed. Secondly, grayscale processing should be performed on the region of interest of the image. Then, the region is segmented based on the preset threshold, and the contour line region image is extracted. Finally, morphological methods were used to process the image, and the centerline of laser welding stripes was extracted through methods such as stripe refinement. Among them, the threshold segmentation of the weld contour image is achieved through binary processing of the image, which mainly filters the pixels in the laser contour image area. Meanwhile, the selection of the binarization algorithm mainly hinges on the grayscale threshold of the pixel, and its calculation is Equation (2).

$$u(x,y) = \begin{cases} 0, & f(x,y) \le T \\ 255, & f(x,y) > T \end{cases} \tag{2}$$

T in Equation (2) represents the grayscale threshold. In image acquisition, the width of the laser emission line will affect that laser stripe. As a result, in identifying feature points, it is necessary to refine the laser welding contour lines. In the definition of stripe refinement, R represents a set of planes. B represents the boundary of the set. P represents a point in the set. The point closest to P on the boundary is M. The union of P points is the skeleton of the set of planes. When performing stripe refinement, it is first necessary to determine the weld contour pixels and skeleton pixels of the plane set R. Next, remove the non skeleton points from the contour pixels, and finally use the remaining skeleton pixels to replace the original plane set. Repeat the above operation until all R are skeleton pixels.In addition, Hough line fitting is required after extracting the centerline of the image. However, the Hough line fitting algorithm mainly uses voting mechanisms for fitting operations, which can lead to the phenomenon of fitting multiple line segments. Therefore, it is necessary to arrange the fitted line segments from left to right, and compute the angle and intersection coordinates of every two adjoining line segments, to achieve more precise recognition

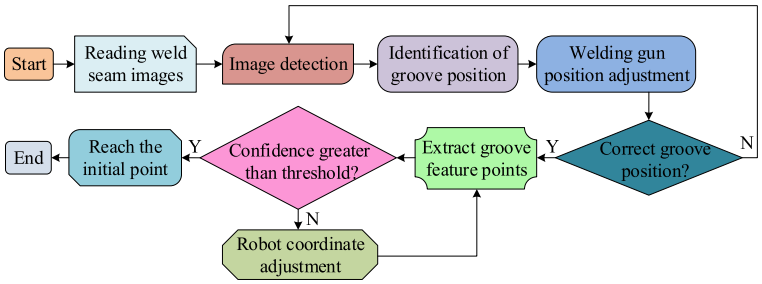

FIGURE 4. The IPP process of the weld seam.

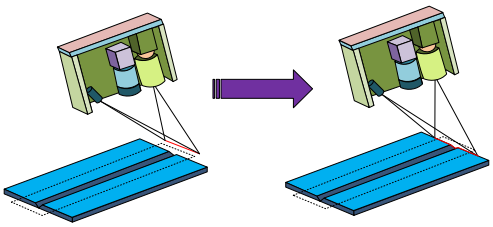

(a) Initial point exploration (b) Exploring the initial point

FIGURE 5. Schematic diagram of structured light seeking the starting point of weld.

of feature points [21], [22]. Among them, the left endpoint $p_1(x_1, y_1)$ represents the left edge of the weld groove, and the middle endpoint $p_2(x_2, y_2)$ is located at the bottom of the weld. The right endpoint $p_3(x_3, y_3)$ represents the right edge of the weld groove. Next, it is necessary to perform feature matching calculations on the identified corner coordinates. The positional coordinate relationship of the feature points is Equation (3).

$$\begin{cases} -t \le y_1 - y_3 \le t \\ -k \le x_2 - (\dfrac{x_1 + x_3}{2}) \le k \end{cases} \tag{3}$$

In Equation (3), t and k represent thresholds.

To locate the initial welding point more accurately, a method combining depth learning prediction with traditional structured light image processing algorithm is introduced. The specific IPP process of the weld seam is Figure 4.

The IPP step of the weld groove is to first use a DL detection camera to capture images, and input them into the deep learning model for detection, to obtain the locationdetails. When the robot moves to a suitable area, the contour of the V-shaped weld is recognized by utilizing a structured light sensor camera. If the sensor fails to detect the contour of the V-shaped weld, the robot will continue to move in the direction of the weld until the sensor detects the contour information. Then, the position information of the feature points at the bottom of the weld seam is identified, and the coordinates of that position are obtained using a hand eye transformation algorithm. Finally, the robot moves to the beginning point of the weld seam according to the obtained position coordinates, thereby completing the IPP process [23]. The specific positioning process diagram is Figure 5.

B. ML-MC WELDING PLANNING BASED ON MACHINE VISION

1) ACQUISITION OF WELD TRACK SECTION PARAMETERS

ML-MC welding mainly includes filling, cover and backing welding. Due to the susceptibility of the cross-sectional area, it is necessary to set welding parameters in advance to meet the needs of different groove widths and angles of the weld bead. Due to the root structure of the weld groove is the weakest position, the quality of the entire ML-MC welding is affected by the quality of the backing weld. Therefore, strict control of welding heat is required when welding the backing layer. If the welding heat is too high, it will increase the fusion ratio of the weld bead, leading to an increase in impurities in the weld metal and the occurrence of cold cracks. If the heat input is too small, the cooling rate of the bottom layer of the plate will be accelerated, which will lead to brittle hard tissue of the weldment structure, and reduce the toughness of the weldment to form cold cracks. In the filling welding of ML-MC, if the input heat is too large, it will increase the thickness of each layer of weld seam, resulting in a decrease in the forming effect of the weld seam and susceptibility to liquefaction cracks. Therefore, the input heat should be reduced to prevent the occurrence of cracks and increase the toughness of the weld seam. The main function of cover welding is to fully cover the groove after filling welding, thereby ensuring the quality of welding formation [24], [25]. The filling area is mainly affected by many parameters such as the current size of the welding machine. The calculation of the welding cladding section area is Equation (4).

$$S = \frac{V_f \pi D_f^2}{4 V_w} \tag{4}$$

In equation (4), V_f represents the wire feeding speed. V_w is the travel speed of the welding machine. D_f is the wire diameter. In the actual welding process of the weld bead, the welding equipment will automatically adjust the welding current, voltage, and wire feeding speed according to the actual situation. The welding voltage is mainly used to supply energy for the melting of the welding wire, and the higher the voltage, the faster the melting speed of the welding wire. The welding current mainly adjusts the balance between the melting speed and wire feeding speed. The cross-sectional area of the weld bead is mainly influenced by multiple factors such as cladding efficiency et al. The welding current and the

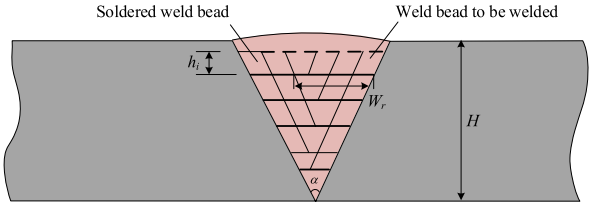

FIGURE 6. Schematic diagram of visual dynamic lane arrangement.

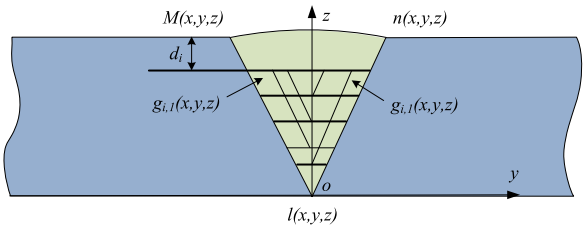

FIGURE 7. Schematic diagram of dynamic lane arrangement coordinate system.

cross-sectional area of the filler layer weld bead were used for data fitting. The results are listed in Equation (5).

$$S = 0.2396 \times I_i - 24.5285 \tag{5}$$

I_i in Equation (5) represents the welding current.

2) VISUAL DYNAMIC ROW PLANNING OF MULTI-LAYER AND MULTI-CHANNEL WELDING PATHS

The path planning method for ML-MC welding usually adopts equal area filling or equal height filling. However, this method's effectiveness during the welding process can be easily impacted by the formation of the weld seam, which can cause issues such as groove deformation, deviation in the welding position of the remaining weld beads, and low welding quality [26]. Therefore, the study introduces visual dynamic routing on the basis of traditional algorithms, which can monitor the groove changes of welds in real-time, thereby achieving path correction of welding. Figure 6 is a schematic diagram of visual dynamic lane arrangement. In Figure 6, h_i and W_r represent the height and width of the weld bead to be welded. H represents the height of the entire weldment, and F represents the angle of the V shaped weld groove. The steps of this method are firstly to use structured light sensors to obtain the actual distribution position of weld bead in the welding process in real time. Next, the obtained parameters should be compared with the planned path of the original weld bead. If it does not exceed the set error range, the next weld bead will be welded according to the original weld bead parameters. If it exceeds the designated error range, adjust the planning of the next weld bead's position in real-time to ensure the filling height of the weld bead matches the actual planning, thus avoiding sharp corners and grooves. In addition, this method achieves effective filling and controllable forming of welds under the influence of various fluctuation parameters, thereby obtaining more ideal welding joints.

The dynamic path arrangement planning of ML-MC welding adopts contour filling. The images are collected by structured light sensors, and the visual algorithm is compiled at the same time. At the same time, it is necessary to detect the angle of the weld groove, the width of the groove, and the thickness of the welded part. Based on these parameters, the height of the remaining welding layer and the width of the filling layer can be calculated. To establish a coordinate system utilizing the cross-section of the welding groove, wherein the x-axis is oriented towards the welding advancement direction; The y-axis indicates the horizontal direction that is perpendicular to the weld seam, and the z-axis is directed towards the thickness of the welded component. The schematic diagram of the V-shaped groove ML-MC dynamic layout coordinate system is Figure 7.

The height of the remaining layer to be welded is calculated as Formula (6).

$$d_i = \frac{d(m_z - g_z)}{m_z} \tag{6}$$

In Equation (6), d represents the height of the welding groove. m_z is the z-axis coordinate of the point along the edge of the groove. g_z represents that of the welding starting point. The width calculation of the filling layer is Equation (7) [27].

$$L' = \frac{(d - d_i)}{\tan(\frac{\pi - \alpha}{2})} \tag{7}$$

In Equation (7), α represents the angle of the weld groove. The number of weld beads to be filled is calculated as Equation (8).

$$n = \frac{L'}{M} \tag{8}$$

In Equation (8), M represents the swing coefficient of the welding. The coordinate positions of each layer of weld bead are displayed in Equation (9).

$$g_{ij}(x, y, z) \Rightarrow \begin{cases} xi_j = x_0 \\ y_{ij} = y_{i1} + j \cdot \Delta y \\ zi_j = z_0 + i \cdot \Delta z \end{cases} \tag{9}$$

In Equation (9), $g_{ij}(x, y, z)$ represents the position coordinates of the i layer and j column of the welding seam. Δy is the width, and Δz is the height. The calculation of the welding height of the remaining filling layer is Equation (10).

$$d_h = d_i - d_k(10) \tag{10}$$

In Equation (10), d_k represents the thickness of the cover layer. The cross-sectional area of the last filling layer is calculated as Equation (11).

$$S_i = \frac{d_h + 2 \cdot (d - d_i)}{\tan(\frac{\pi - \alpha}{2})} \times d_h \tag{11}$$

The area calculation of the diamond weld bead is Equation (12).

$$S_r = d_h \times M \tag{12}$$

The planned number of weld beads for this diamond shaped weld bead layer is calculated as Equation (13).

$$n'' = \frac{S_i}{S_r} \tag{13}$$

The calculation of welding current is Equation (14).

$$V_w = \frac{24.5285 + S_r}{0.2386} \tag{14}$$

If the measured coordinate error of the weld bead exceeds the established range, it is necessary to perform a secondary pass arrangement within the welding layer. The coordinates of the secondary pass arrangement appear in Equation (15) [28].

$$g_{ij}(x, y, z) \Rightarrow \begin{cases} xi_j = x_0 \\ y_{ij} = y_{ic} + j \cdot \Delta y \\ zi_j = z_0 + i \cdot \Delta z \end{cases} \tag{15}$$

In Equation (15), y_{ic} represents the y-axis coordinate of the c-th weld bead of layer i. In actual welding operations, the main focus is on accurately identifying the contour feature point positions of the weld seam. The study selected medium and thick plate welding workpieces for multi-layer and multi pass welding experiments. To optimize contour collection and save workpieces during welding, a bottom-to-top approach is utilized. This method facilitates contour gathering for every weld seam. The cladding forming images of different welding layers are collected by structured light vision sensor. To collect the cladding profile image under the same weld condition and save welding materials, the research will weld the same weld, and use structured light sensors to collect images of weld beads with different lengths. Usually, different welding layers exhibit different shape characteristics. The base layer takes a clear "V" shape, while the filling layer displays distinct contour, edge, and corner characteristics, particularly at the weld/cladding intersection. In the algorithm for identifying the bottom of the weld groove, it is first acquired to reduce the length parameter threshold of the fitting line to fit more weld contour lines. Simultaneously, it needs to set the angle threshold between adjacent lines and calculate the corner position of the fitted line. Next, it is necessary to record the coordinates of the four intersection points in the image from left to right in order to obtain the trench bottom feature points of the underlying layer. Among them, the two intersections in the middle represent the characteristic points of the filling layer, and the intersections at both ends represent the left and right edge points of the weld groove. Finally, the corresponding weld path is determined by utilizing the height and width of the weld seam and the distribution information of feature points within the filling layer. This approach achieves ML-MC welding dynamic routing of the weld groove [29], [30]. The specific process of dynamic routing for ML-MC is Figure 8.

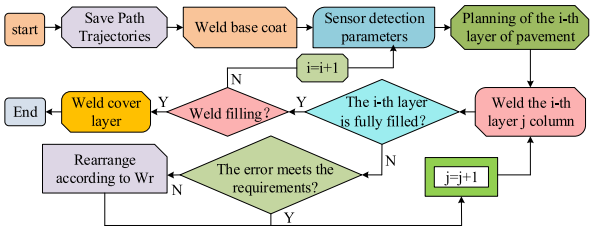

FIGURE 8. The specific process of dynamic routing for ML-MC welding.

TABLE 1. Table of initial point prediction coordinates of weld joint.

Order number	Shot confidence	Feature point confidence	Positioning coordinates	Deviation from ideal area
1	0.88	0	(824,1072)	(676,2428)
2	0.91	0	(1042,2546)	(458,954)
3	0.93	0	(1107,2931)	(393,569)
4	0.95	0	(1235,3317)	(265,183)
5	0.98	1	(1300,3420)	(200,80)

IV. APPLICATION ANALYSIS OF ML-MC DYNAMICROUTINGPLANNING AND IPP GROUNDED ON MACHINE VISION

In the experiment to verify the relationship between MV-ML-MC-DRP and weld IPL, a TCP communication server was used as the recognition system software to achieve interactive data transmission. TCP communication client is set as the system software for dynamic programming of weld seam routing and IPP of weld seam. To verify the effectiveness of weld IPL, the study first used YOLOv3's already trained DL model to identify the position of the weld groove and roughly locate the initial point of the weld. Then the SLV is utilized to determine the confidence of the weld contour. Then, SLV is used to determine the confidence of weld contour. The confidence of weld detection refers to the probability or reliability that the system believes that a detected weld is correct. Confidence is one of the important indicators for evaluating the performance of detection algorithms. When the confidence level is greater than the set threshold, the current initial point of the weld seam is located and the welding robot is adjusted to IPP. As the confidence level changes, the coordinate information of the weld seam changes as Table 1. The difference between the coordinates determined by the DL model and the optimal area decreases gradually, with a minimum of (200,80). Moreover, the confidence level of weld seam detection gradually increased, reaching a maximum of 98%, and the confidence level of detected feature points reached 100%. This shows that the model and SLV have high detection accuracy and performance advantages.

The study then proceeded to measure the distance between the start point of the weld seam and the tip of the wire after positioning the system. This involves measuring the horizontal distance Δx and vertical distance Δy between the two endpoints, and determining the error for both values using the collinear theorem. The superiority of the SLV is verified through experimental comparison and analysis with current advanced stereo vision algorithms. Figure 9 displays the measured values for horizontal and vertical

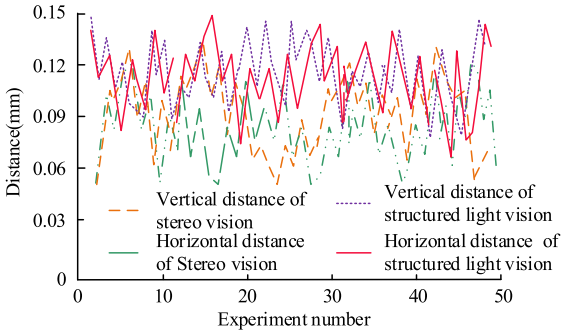

(a) Horizontal and vertical distance of visual sensing positioning

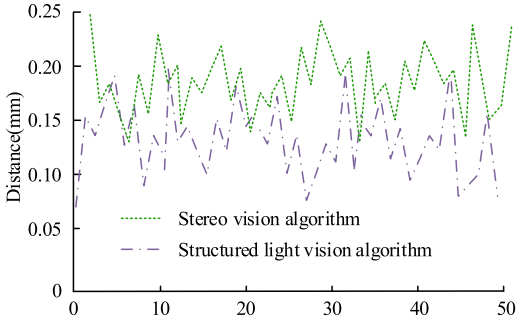

(b) Visual sensing positioning error

FIGURE 9. Horizontal and vertical distance and error value results.

distance deviation and error after 50 sets of experiments. From Figure 9(a) in the SLV, the initial point of the welding robot has a maximum deviation of 0.12 mm in the horizontal direction. The minimum deviation is only 0.05 mm, resulting in a reduction of deviation values by 0.03 mm and 0.01 mm when compared to the stereo vision algorithm. At the same time, the initial point of the SLV in the vertical direction has a maximum deviation of 0.13 mm, and the minimum deviation value is only 0.05 mm. Compared with the stereo scopic vision algorithm, the maximum deviation is 0.13 mm. Compared with the stereo vision algorithm, the deviation values are reduced by 0.03mm and 0.03mm, respectively. From Fig. 9(b), the maximum error of the SLV is 0.20mm, and the minimum error is only 0.07mm. Compared with the stereo vision algorithm, the error values are reduced by 0.05mm and 0.04mm, respectively. This shows that compared with the stereo vision algorithm, the SLV has a higher positioning accuracy for positioning the initial welding point.

Research continues to validate the effective performance of the dynamic routing algorithm for machine learning-based multitask welding. The experiment initially identifies the feature points' location, calculates their position data relative to the welding robotic arm, and acquires the weld seam path. Next, it identifies the position coordinates of the contour feature points of the weld seam in the image, and pre plans the welding path based on the calculated welding current value. Finally, the study aims to achieve welding of the base layer in accordance with the weld path and to identify the contour feature points of the weld repeatedly during the welding of

TABLE 2. Pre planned welding parameters for each weld bead before welding.

Sequence	Type	Welding speed (cm/min)	Welding gun inclination angle (°)	Current value (A)
1	Backing welding	30	0	290
2	FW 1	30	0	230
3	FW 1	30	-20	200
4	FW 2	30	20	230
5	FW 2	30	-20	210
6	FW 2	30	20	230
7	CW	30	0	220
8	CW	30	0	220

*Note: FW means Filler welding; CW means Capping welding.

TABLE 3. Average error results for each channel weld.

Algorithm	ME	RMSE
Visual dynamic routing algorithm	3.58	1.15
Traditional algorithm	20.14	15.22

the cover and filling layers. Table 2 is the pre planned welding parameters for each weld bead before welding.

Further research was conducted to verify the effectiveness of the visual dynamic routing algorithm for multi-layer and multi-pass welding, and ablation experiments were conducted on it. Experimental comparison was conducted between traditional welding techniques and welding techniques based on visual dynamic routing algorithms. The pixel error analysis indicators of weld feature points are Maximum Error (ME) and Root-mean-square deviation (RMSE). The average error results of each weld seam are shown in the Table 3. From the Table 3, it can be seen that compared to traditional welding techniques, welding techniques based on visual dynamic routing algorithms have lower feature point recognition errors. The ME value of each weld seam is only 3.58, a decrease of 16.56 compared to traditional algorithms. And its RMSE value is only 1.15, which is 14.07 lower than traditional algorithms. The visual dynamic routing algorithm for multi-layer and multi-pass welding has significant performance advantages.

The structured light camera is used to recognize the weld contour and extract the position coordinates of its feature points, so that the required weld information can be obtained. The contour feature points' recognition results during welding are shown in Figure 10. As the filling layer continues to increase, the positions of the two feature points in the middle continue to move up, while the remaining width of the welding layer gradually decreases. At this point, the width of the feature points of the two filling layers in the middle continuously changes as the number of filling layers increases.

The width of feature points and the remaining width of the welding layer obtained through visual system recognition are listed in Figure 11. As the welded area expands, the width of its distinctive points and the residual width of the welded layer fluctuate continuously. Among them, the fluctuation range of the feature points is 59mm-138mm, and

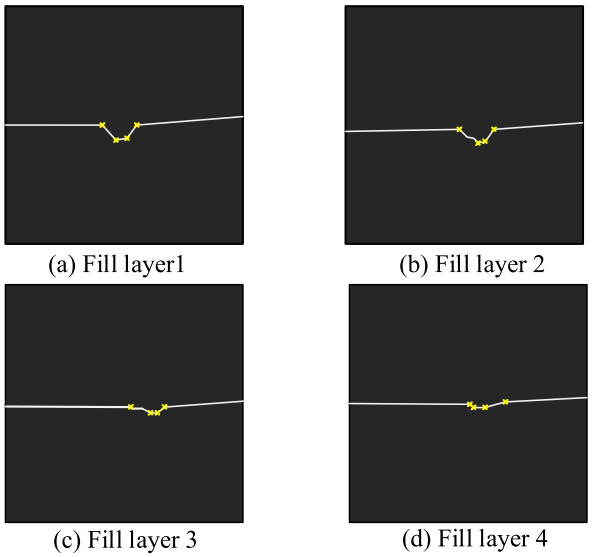

FIGURE 10. Recognition results of contour feature points during welding process.

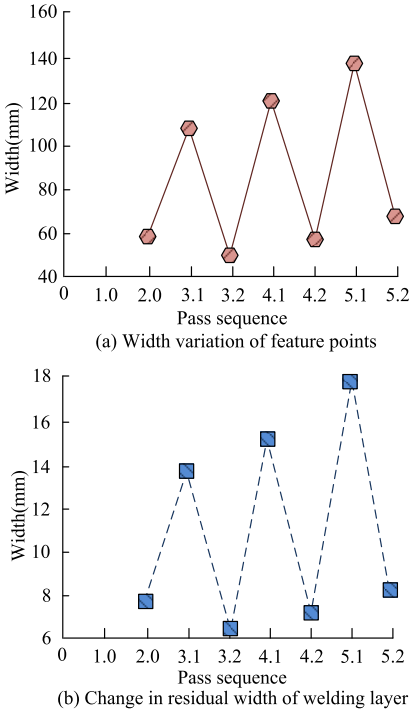

FIGURE 11. Feature points and residual width information of welding layer.

the fluctuation range of the remaining width of the welding layer is 6.189mm-17.462mm. By utilizing the dynamic routing planning algorithm for ML-MC welding, the visual sensing system provides feedback to the welding robot regarding the relevant welding layer width and weld bead width data. The welding equipment will adjust its current and welding position for the following layer using feedback data. This allows for efficient scheduling and planning of ML-MC welding.

The welding path of the backing weld is obtained by scanning the welding visual sensor, while the welding trajectory

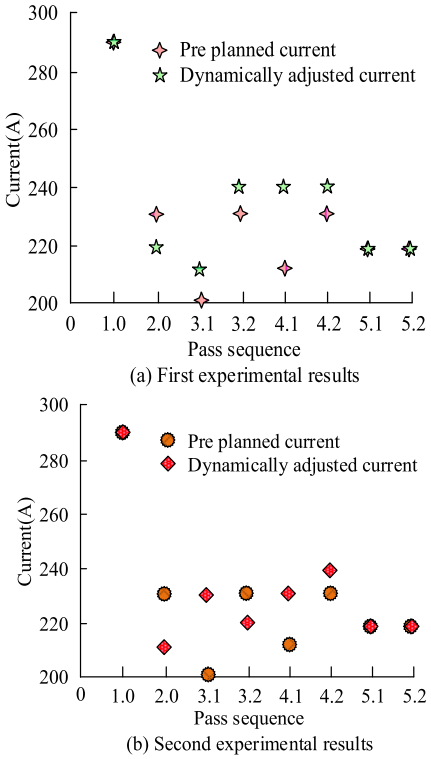

FIGURE 12. Comparison of current values between dynamic programming and pre planning.

of the cover weld and fill weld is obtained by dynamically offsetting the backing weld layer. The comparison results of two groups of experiments with the welding current obtained after dynamic programming and the pre planned current value are shown in Figure 12. After dynamic adjustment of the current value, the current values of each filling welding layer have deviations from the pre planned current values, with the maximum current deviation reaching 30A. The dynamic adjustment current values of the base welding and each cover welding are completely consistent with the pre planned current values. This indicates that in the actual welding process, the welding robot will adjust the current based on real-time detection data from visual sensors, thereby achieving more accurate welding operations.

To verify the practical application effect of machine vision based dynamic routing welding method, the paper will conduct actual inspection on the welded parts after welding using this method. After completing the welding of each layer, the cross-section is first polished, and then corroded with a 4% nitric acid solution to obtain that of the weld bead. The entire welding time is 15-20min. The relationship between weld cross-sectional area and current for each weld layer at different welding speeds and the relationship between weld current and weld cross-sectional area for the filler layer are shown in Fig. 13. The cross-sectional area of the weld bead is mainly affected by the welding speed and welding current. The cross-sectional area deducts with the rise of welding speed and rises with the welding current booming. When the current is 291A and the welding speed is 30cm/min, the cross-sectional area reaches the maximum

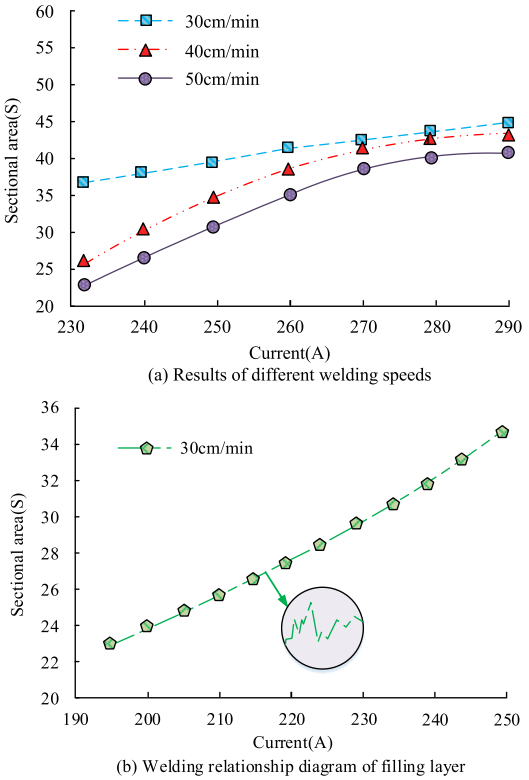

FIGURE 13. Relationship diagram between welding current and weld bead cross-sectional area.

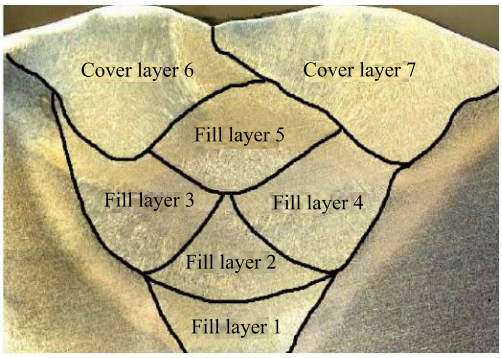

FIGURE 14. Cross section view of welded workpiece.

value of 44.5mm^2. In addition, the growth rate of that area of the filling layer is faster than that of the other welding layers. This shows that welding speed and welding current play a crucial role in the quality of the filler layer. It is therefore necessary to adjust the welding speed and welding current to the optimum using vision sensors.

The experiment continued to conduct 4-layer and 8-pass welding on the welded parts to verify their actual effect. The welding cross-section image after corrosion treatment is exhibited in Figure 14. This welding treatment includes 5 filling layers and 2 cover layers. After actual measurement, the remaining height of the fusion after welding is 2.5mm. There are no adverse phenomena such as undercut, incomplete penetration, slag inclusion, and porosity on the weld-seamsurface. This indicates that the overall welding quality fully meets practical needs and can be applied to actual welding engineering. In actual welding, the dynamic routing welding method not only improves production quality, but also simplifies the routing algorithm, thereby improving production efficiency.

V. CONCLUSION

The filling quality of welding is the most critical element in the entire process. To further lift the filling quality of ML-MC, CNN and structured light imaging method of V-shaped weld groove are introduced to precisely locate the initial point of weld groove. At the same time, the paper also designed MV-ML-MC-DRP and contour feature point recognition algorithms for filling layers to dynamically schedule welding for ML-MC welding. The results show that in the initial point localization experiments, the maximum deviation value of the initial point of the welding robot in the horizontal direction within the SLV is 0.12 mm, and the minimum deviation value is only 0.05 mm. Compared with the stereo vision algorithm, the deviation values are reduced by 0.03 mm and 0.01 mm, respectively. Moreover, the maximum matching deviation of the initial point in the vertical direction in the SLV value is 0.13mm and the minimum deviation value is only 0.05mm. Compared to the stereo vision algorithm, the deviation values are reduced by 0.03mm and 0.03mm, respectively. Meanwhile, the maximum error of the SLV is 0.20mm and the minimum error is only 0.07mm. Compared to the stereo vision algorithm, the error values are reduced by 0.05mm and 0.04mm, respectively. In the recognition verification of the visual system, the width of feature points and the remaining width of the welding layer continuously fluctuate up and down as the welding layer increases. The fluctuation range of feature points is 59mm-138mm, and the fluctuation range of the remaining width of the welding layer is 6.189mm-17.462mm. Among them, when the current is 291A and the welding speed is 30cm/min, the cross-sectional area of the filler layer reaches the max of 44.5mm^2. It shows that the welding system based on machine vision has good practical application effect and meets the process requirements of welding. At the same time, the welding technology effectively improves the welding accuracy and welding quality, and promotes the automation and intelligent development of welding technology. However, this study did not optimize the design of the welding robot control system, which is an important part of the robot welding system. Therefore, subsequent research can improve the control accuracy and response speed of the robot by introducing advanced control algorithms and optimisation methods.

REFERENCES

[1] M. Zhu, W. Wu, W. Qian, L. Xia, Y. Zhang, and B. Wang, "A brief review on welding of stainless steel clad plates: Issues and future perspectives," *Int. J. Adv. Manuf. Technol.*, vol. 115, nos. 1–2, pp. 49–59, Jul. 2021, doi: 10.1007/s00170-021-07218-9.

[2] W. Winarto, H. Oktadinata, D. Priadi, A. Baskoro, and K. Ito, "Microstructure and impact toughness relationship for different nickel level of electrode in multi-pass FCA welded SM570-TMC steel joint," *Quart. J. Jpn. Weld. Soc.*, vol. 38, no. 2, pp. 154–158, Jan. 2020, doi: 10.2207/qjjws.38.154s.

[3] O. Y. Sergiyenko and V. V. Tyrsa, "3D optical machine vision sensors with intelligent data management for robotic swarm navigation improvement," *IEEE Sensors J.*, vol. 21, no. 10, pp. 11262–11274, May 2021, doi: 10.1109/JSEN.2020.3007856.
[4] Y. Song, Z. Xie, X. Wang, and Y. Zou, "MS-YOLO: Object detection based on YOLOv5 optimized fusion millimeter-wave radar and machine vision," *IEEE Sensors J.*, vol. 22, no. 15, pp. 15435–15447, Aug. 2022, doi: 10.1109/JSEN.2022.3167251.
[5] J. Fan, S. Deng, F. Jing, C. Zhou, L. Yang, T. Long, and M. Tan, "An initial point alignment and seam-tracking system for narrow weld," *IEEE Trans. Ind. Informat.*, vol. 16, no. 2, pp. 877–886, Feb. 2020, doi: 10.1109/TII.2019.2919658.
[6] S. Trupiano, V. G. Belardi, P. Fanelli, L. Gaetani, and F. Vivio, "A novel modeling approach for multi-passes butt-welded plates," *J. Thermal Stresses*, vol. 44, no. 7, pp. 829–849, Jul. 2021, doi: 10.1080/01495739.2021.1916415.
[7] R. K. W. Vithanage, E. Mohseni, Z. Qiu, C. MacLeod, Y. Javadi, N. Sweeney, G. Pierce, and A. Gachagan, "A phased array ultrasound roller probe for automated in-process/interpass inspection of multipass welds," *IEEE Trans. Ind. Electron.*, vol. 68, no. 12, pp. 12781–12790, Dec. 2021, doi: 10.1109/TIE.2020.3042112.
[8] M. Zhu, Q. Zheng, W. Wu, W. Qian, Y. Zhang, and B. Wang, "Influence of welding sequence on residual stress evolution in Incoloy825/X52 bimetallic clad plate butt-welded joints," *Sci. Technol. Weld. Joining*, vol. 26, no. 5, pp. 356–362, Jul. 2021, doi: 10.1080/13621718.2021.1916227.
[9] Y. Han, B. Kong, J. Wang, K. Fu, H. Jin, J. Chen, and Y. Wei, "Effect of laser-arc heat input ratio on the formation, microstructure, and properties of EH36 steel with laser-metal inert gas hybrid welding," *J. Mater. Eng. Perform.*, vol. 32, no. 4, pp. 1954–1965, Feb. 2023, doi: 10.1007/s11665-022-07203-7.
[10] A. Sarmast, J. Schubnell, and M. Farajian, "Finite element simulation of multi-layer repair welding and experimental investigation of the residual stress fields in steel welded components," *Weld. World*, vol. 66, no. 6, pp. 1275–1290, Jun. 2022, doi: 10.1007/s40194-022-01286-5.
[11] M. Shahabi, H. Ghariblu, M. Beschi, and N. Pedrocchi, "Path planning methodology for multi-layer welding of intersecting pipes considering collision avoidance," *Robotica*, vol. 39, no. 6, pp. 945–958, Jun. 2021, doi: 10.1017/S026357472000082X.
[12] L. H. Guilherme, A. V. Benedetti, C. S. Fugivara, R. Magnabosco, and M. F. Oliveira, "Effect of MAG welding transfer mode on sigma phase precipitation and corrosion performance of 316L stainless steel multi-pass welds," *J. Mater. Res. Technol.*, vol. 9, no. 5, pp. 10537–10549, Sep. 2020, doi: 10.1016/j.jmrt.2020.07.039.
[13] Y. He, G. Ma, and S. Chen, "Autonomous decision-making of welding position during multipass GMAW with T-joints: A Bayesian network approach," *IEEE Trans. Ind. Electron.*, vol. 69, no. 4, pp. 3909–3917, Apr. 2022, doi: 10.1109/TIE.2021.3076710.
[14] N. Mukai, Y. Inoue, S. Sasakura, and Y. Kinoshita, "Prevention of cold cracking by the welding process for reducing diffusible hydrogen in high-tensile thick plate welding," *Weld. Int.*, vol. 33, nos. 7–9, pp. 268–280, Sep. 2019, doi: 10.1080/09507116.2020.1866362.
[15] M. Hasan Al-Hafadhi and G. Krallics, "Prediction and numerical simulation of residual stress in multi-pass pipe welds," *Pollack Periodica*, vol. 16, no. 2, pp. 7–12, Jun. 2021, doi: 10.1556/606.2020.00127.
[16] P. Asadi, S. Alimohammadi, O. Kohantorabi, A. Soleymani, and A. Fazli, "Numerical investigation on the effect of welding speed and heat input on the residual stress of multi-pass TIG welded stainless steel pipe," *Proc. Inst. Mech. Eng. B, J. Eng. Manuf.*, vol. 235, nos. 6–7, pp. 1007–1021, May 2021, doi: 10.1177/0954405420981335.
[17] E. Kolakowska, S. F. Smith, and M. Kristiansen, "Constraint optimization model of a scheduling problem for a robotic arm in automatic systems," *Robot. Auto. Syst.*, vol. 62, no. 2, pp. 267–280, Feb. 2014, doi: 10.1016/j.robot.2013.09.005.
[18] M. Foumani, I. Gunawan, and K. Smith-Miles, "Increasing throughput for a class of two-machine robotic cells served by a multifunction robot," *IEEE Trans. Autom. Sci. Eng.*, vol. 14, no. 2, pp. 1150–1159, Apr. 2017, doi: 10.1109/TASE.2015.2504478.
[19] S. Yu, Y. Guan, Z. Yang, C. Liu, J. Hu, J. Hong, H. Zhu, and T. Zhang, "Multiseam tracking with a portable robotic welding system in unstructured environments," *Int. J. Adv. Manuf. Technol.*, vol. 122, nos. 3–4, pp. 2077–2094, Sep. 2022, doi: 10.1007/s00170-022-10019-3.
[20] J. Gao, Y. Hong, B. Hong, X. Li, A. Jia, and Y. Qu, "A method of feature extraction of position detection and weld gap for GMAW seam tracking system of fillet weld with variable gaps," *IEEE Sensors J.*, vol. 21, no. 20, pp. 23537–23550, Oct. 2021, doi: 10.1109/JSEN.2021.3106696.
[21] Z. Zhao, J. Luo, Y. Wang, L. Bai, and J. Han, "Additive seam tracking technology based on laser vision," *Int. J. Adv. Manuf. Technol.*, vol. 116, pp. 197–211, Jun. 2021, doi: 10.1007/s00170-021-07380-0.
[22] M. Giordani and M. Zorzi, "Non-terrestrial networks in the 6G era: Challenges and opportunities," *IEEE Netw.*, vol. 35, no. 2, pp. 244–251, Mar./Apr. 2021, doi: 10.1109/MNET.011.2000493.
[23] W. Fang, X. Xu, and X. Tian, "A vision-based method for narrow weld trajectory recognition of arc welding robots," *Int. J. Adv. Manuf. Technol.*, vol. 121, nos. 11–12, pp. 8039–8050, Aug. 2022, doi: 10.1007/s00170-022-09804-x.
[24] S.-T. Mi, Y.-C. Zhang, X.-B. Fu, F. Yan, and J.-L. Shen, "A measurement method of weld temperature and tool positioning during friction stir welding process," *Weld. World*, vol. 65, no. 8, pp. 1531–1540, Apr. 2021, doi: 10.1007/s40194-021-01067-6.
[25] K. Biester, L. Budde, A. Barroi, M. Lammers, J. Hermsdorf, and L. Overmeyer, "Investigation of deposition welding in vertical and horizontal position with a coaxial laser wire welding head," *Int. J. Adv. Manuf. Technol.*, vol. 120, nos. 7–8, pp. 5399–5410, Jun. 2022, doi: 10.1007/s00170-022-09013-6.
[26] N. P. Nguyen, M. Brosda, A. Olowinsky, and A. Gillner, "Absorber-free quasi-simultaneous laser welding for microfluidic applications," *J. Laser Micro Nanoeng.*, vol. 14, no. 3, pp. 255–261, 2019, doi: 10.2961/jlmn.2019.03.0009.
[27] P. Zhou, R. Peng, M. Xu, V. Wu, and D. Navarro-Alarcon, "Path planning with automatic seam extraction over point cloud models for robotic arc welding," *IEEE Robot. Autom. Lett.*, vol. 6, no. 3, pp. 5002–5009, Jul. 2021, doi: 10.1109/LRA.2021.3070828.
[28] L. Chen, G. Liu, S. Li, Y. Mo, Z. Han, X. Liang, and H. Pan, "A novel 8-shape trajectory weaving welding control algorithm with auto-adjust welding torch attitude," *Int. J. Adv. Manuf. Technol.*, vol. 120, nos. 11–12, pp. 8377–8387, Apr. 2022, doi: 10.1007/s00170-022-09225-w.
[29] J. Ge, Z. Deng, Z. Li, W. Li, T. Liu, H. Zhang, and J. Nie, "An efficient system based on model segmentation for weld seam grinding robot," *Int. J. Adv. Manuf. Technol.*, vol. 121, nos. 11–12, pp. 7627–7641, Aug. 2022, doi: 10.1007/s00170-022-09758-0.
[30] K. M. Heide, S. Heikebrügge, C. Dänekas, B. Breidenstein, and P. Schaumann, "Automated geometry measurement and deep rolling of butt welds," *Weld. World*, vol. 66, no. 12, pp. 2533–2547, Dec. 2022, doi: 10.1007/s40194-022-01346-w.

TONG LI received the bachelor's degree in welding technology and equipment from the Sichuan Institute of Technology, in 1998, and the master's degree in materials processing engineering from Chongqing University, in 2005. He is currently a senior experimenter. He is also with Xihua University, mainly engaged in research on automation and intelligent welding. He have published five academic articles, participated in more than 20 scientific research projects, authorized seven patents, and won one second prize of Sichuan Provincial Science and Technology Progress Award.

JIANG ZHENG received the bachelor's degree in mechanical and electronic engineering from Xihua University, in 2020. He is currently pursuing the master's degree. He is also mainly engaged in research in the fields of automation and intelligent welding.